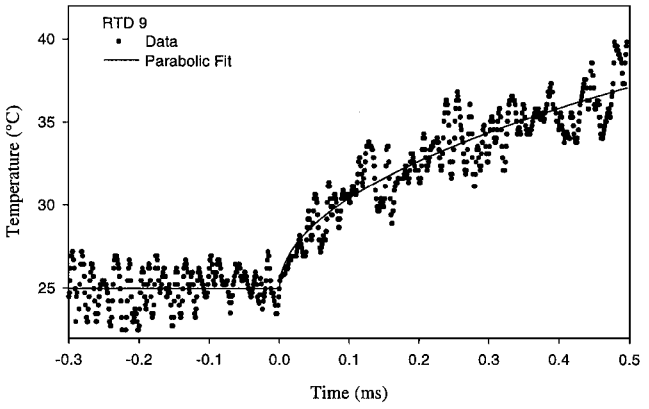

a) Least-squares parabolic fit for $t \geq 0$

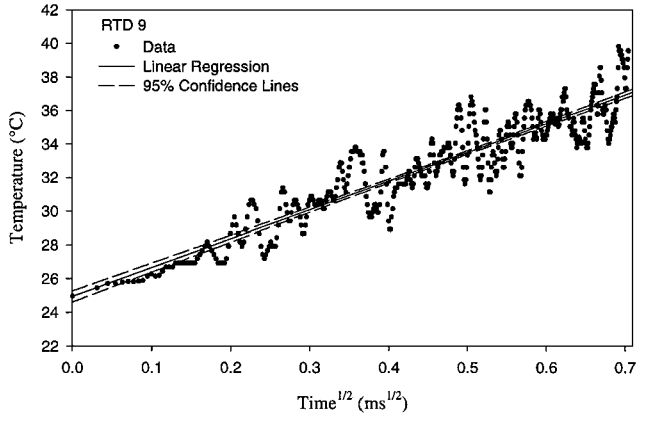

b) Data replotted against the square root of time elapsed from start of heating

Fig. 3 Temperature response of RTD subjected to an impinging shock.

where the slope λ is obtained from a least-squares regression to the data in Fig. 3b for $t \geq 0$. For this particular RTD, $\dot{q}_s = 23.2$ W/cm^2 $\pm$ 11%.

From Fay–Riddell theory, the stagnation-point heat flux for perfect gas flow past a hemispherical probe is[6]

$$\dot{q}_{t,\text{ref}} = \frac{0.763}{(Pr_{w,t})^{0.6}}(\rho_{t2}\mu_{t2})^{0.4}(\rho_{w,t}\mu_{w,t})^{0.1} \times (H_{t2} - h_{w,t})\left[\frac{1}{R_N}\sqrt{\frac{2(p_{t2} - p_\infty)}{\rho_{t2}}}\right]^{0.5} \tag{10}$$

where p, ρ, and μ are the pressure, density, and viscosity; H and h are the stagnation and static enthalpy; Pr is the Prandtl number; and R_N is the nose radius. The subscripts t_2 denote stagnation conditions downstream of a normal shock, w the surface conditions, t the stagnation-point value, and ∞ the freestream conditions. The analysis yields $\dot{q}_{t,\text{ref}} = 26.2$ W/cm^2 $\pm$ 3%. Thus, the experimental values were within 11% from theory and within acceptable accuracy margins.

Conclusion

Resistance temperature detectors are reliable and rugged and thus suitable for use in transient facilities. Self-heating tests showed that ohmic heating is almost zero up to an excitation of about 1 V and that its effect can be accounted for in the final calculations for excitation values up to 2 V. However, an inexpensive and convenient dynamic calibration technique utilizing self-heating was found to be feasible. Dynamic calibrations indicated that a short pulse between 5 and 10 V was adequate for obtaining accurate thermal product values. Experiments showed that handmade thin-film gauges can be used to accurately measure heat flux in transient facilities.

Acknowledgments

This research was supported by the NASA/University of Texas at Arlington Center for Hypersonic Research, NASA Grant NAGW 3714, and Lockheed Martin Tactical Aircraft Systems through Purchase Order 4286428, "Development of Hypersonic Technologies."

References

[1]Schultz, D. L., and Jones, T. V., "Heat-Transfer Measurements in Short-Duration Hypersonic Facilities," AGARDograph 163, Feb. 1973.

[2]Carslaw, H. S., and Jaeger, J. C., "The Infinite and Semi-Infinite Solid," *Conduction of Heat in Solids*, 2nd ed., Clarendon, Oxford, 1959, pp. 75, 76.

[3]Cook, W. J., and Felderman, E. J., "Reduction of Data from Thin-Film Heat-Transfer Gauges: A Concise Numerical Technique," *AIAA Journal*, Vol. 4, No. 3, 1966, pp. 561, 562.

[4]Kinnear, K. M., and Lu, F. K., "Design, Calibration and Testing of Transient Thin Film Heat Transfer Gauges," AIAA Paper 98-2504, 1998.

[5]Ligrani, P. M., Camci, C., and Grady, M. S., "Thin Film Heat Transfer Gage Construction and Measurement Details," von Kármán Inst., TM33, Rhode Saint Genese, Belgium, Nov. 1982.

[6]Bertin, J. J., "Stagnation-Region Flowfield," *Hypersonic Aerothermodynamics*, AIAA, Washington, DC, 1994, pp. 249–255.

Determination of the Time Constants of Integrating Spheres Using Monte Carlo Simulation

Zhaoyan Zhang*
Pennsylvania State University,
University Park, Pennsylvania 16802

Introduction

INTEGRATING spheres have been widely used in the measurements of radiative properties; e.g., Kneissl and Richmond,[1] Bober,[2] and Zhang and Modest[3] have measured hemispherical, spectral reflectance of ceramics with integrating spheres together with lasers. The general theory of the integrating sphere for hemispherical spectral reflectance measurements has been provided by Jacquez and Kuppenheim.[4] They formulated the multiple reflections in a cavity as an integral equation and solved the equation for a few cases. In their theory and subsequent applications, it was assumed that the radiation coming out of an integrating sphere instantaneously reached steady state. Because the speed of light is roughly 3×10^8 m/s and the dimension of an integrating sphere usually is around 0.1 m or less, the time constant for an integrating sphere is of the order of nanoseconds. With the development of laser technology, nanosecond Q-switched lasers are commercially available. Scientists have started to look into the radiative properties associated with nanosecond laser–material interactions. It brings up the question of what the limit of an integrating sphere is.

In this study, a Monte Carlo code is developed to simulate the radiation transport inside an integrating sphere. The time constant of the integrating sphere is derived by fitting the transient radiative intensity leaving the sphere with an exponential function.

Problem Formulation and Simulation Results

It is assumed that we have a topological sphere with two apertures, as shown in Fig. 1. One aperture is on the side wall; another one is on the top. The aperture on the side wall is the detector port,

Received 26 February 1999; revision received 25 June 1999; accepted for publication 26 June 1999. Copyright © 1999 by the American Institute of Aeronautics and Astronautics, Inc. All rights reserved.

*Graduate Student, Department of Mechanical Engineering; zyz@michelle.me.psu.edu.

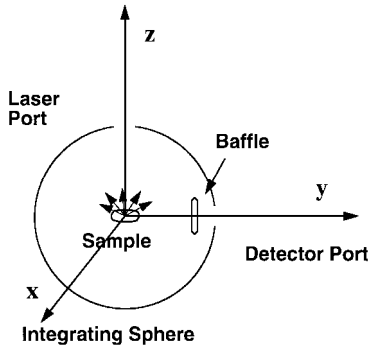

Fig. 1 Schematic of an integrating sphere.

from which a detector can measure the radiative intensity leaving the sphere. Directly in front of the detector port, there is a baffle that is slightly larger than the detector port. The purpose of the baffle is to ensure that no reflected radiation from the sample can leave the integrating sphere without hitting the sphere wall first. The aperture on the top is the entrance port, through which a laser beam can pass. A sample, which is of negligible size, is placed at the center of the sphere. The configuration of the sphere is such that we can compare our steady-state Monte Carlo results with analytical results provided by Jacquez and Kuppenheim.[4]

Surface Description

A spherical coordinate system is set up in vectorial form, with its y axis passing through the center of the baffle. The sphere surface can be described by

$$\boldsymbol{r} = r_0 \sin\theta \cos\phi \boldsymbol{i} + r_0 \sin\theta \sin\phi \boldsymbol{j} + r_0 \cos\theta \boldsymbol{k} \tag{1}$$

where θ is the polar angle from the z axis $[0, \pi]$, ϕ is the azimuthal angle from the x axis $[0, 2\pi]$, and r_0 is the radius of the sphere. For a circular baffle in the plane $y = y_0$, the baffle surface can be described by

$$\boldsymbol{r} = (y_0/\tan\phi)\boldsymbol{i} + y_0 \boldsymbol{j} + [y_0/(\tan\theta \sin\phi)]\boldsymbol{k} \tag{2}$$

We may define two unit tangents to the surface of the sphere and baffle at any points $\boldsymbol{t}_1$ and $\boldsymbol{t}_2$ as

$$\boldsymbol{t}_1 = \frac{\partial \boldsymbol{r}/\partial\theta}{|\partial \boldsymbol{r}/\partial\theta|}, \qquad \boldsymbol{t}_2 = \frac{\partial \boldsymbol{r}/\partial\phi}{|\partial \boldsymbol{r}/\partial\phi|} \tag{3}$$

It can be shown that the surface tangents are perpendicular to each other in our case. The surface normal $\boldsymbol{n}$ can be evaluated as

$$\boldsymbol{n} = \boldsymbol{t}_1 \times \boldsymbol{t}_2 \tag{4}$$

The surface tangents have been arranged such that $\boldsymbol{n}$ is the inward surface normal. For the surface of the sphere, it is found that

$$\boldsymbol{t}_{1,s} = \cos\theta \cos\phi \boldsymbol{i} + \cos\theta \sin\phi \boldsymbol{j} - \sin\theta \boldsymbol{k} \tag{5}$$

$$\boldsymbol{t}_{2,s} = \sin\phi \boldsymbol{i} + \cos\phi \boldsymbol{j} \tag{6}$$

$$\boldsymbol{n}_s = -\sin\theta \cos\phi \boldsymbol{i} - \sin\theta \sin\phi \boldsymbol{j} - \cos\theta \boldsymbol{k} \tag{7}$$

For the baffle surface, it is found that

$$\boldsymbol{t}_{1,b} = \boldsymbol{i}, \qquad \boldsymbol{t}_{2,b} = \boldsymbol{k}, \qquad \boldsymbol{n}_b = \pm \boldsymbol{j} \tag{8}$$

When the baffle surface is facing outward, $\boldsymbol{n}_b$ takes the positive value. It takes the negative value when the baffle surface is facing inward.

Monte Carlo Relations

In the Monte Carlo method a large number of photon bundles are traced from their origins to the next points of intersection. To obtain statistically meaningful results, a relation between the random number generator and the direction of reflection needs to be developed. Assume all of the surfaces are diffuse reflector and absorber. The direction of reflection is independent of the direction of incident radiation. It follows that[5]

$$\theta' = \arcsin\left(\sqrt{R_\theta}\right), \qquad \phi' = 2\pi R_\phi \tag{9}$$

where R_θ and R_ϕ are the random numbers, θ' is the polar angle measured from the local surface normal, and ϕ' is azimuthal angle measured from surface tangent $\boldsymbol{t}_1$. The direction vector $\boldsymbol{s}$ can be derived as

$$\boldsymbol{s} = \sin\theta'(\cos\phi' \boldsymbol{t}_1 + \sin\phi' \boldsymbol{t}_2) + \cos\theta' \boldsymbol{n} \tag{10}$$

The intersection point of a photon bundle reflected at location $\boldsymbol{r}_0$ that traveled into direction $\boldsymbol{s}$ and intersecting surface at location $\boldsymbol{r}$ may be determined as

$$\boldsymbol{r}_0 + D\boldsymbol{s} = \boldsymbol{r} \tag{11}$$

where D is the distance traveling by the photon bundle. The equation can be solved in a three-dimensional domain to determine the three unknowns, D, θ, and ϕ.

Numerical Algorithm

A large number of photon bundles are generated for a small time interval. The number of photon bundles generated in each time interval is proportional to the transient intensity of the laser irradiation. Each of these photon bundles has a time tag to specify the time at which it is generated. When the photon bundle hits the sample surface in the center, it is reflected with a statistical weight of $(1 - \alpha_s)$, where α_s is the absorptance of the sample. The direction of reflection is specified by θ' and ϕ'. The photon bundle may be intercepted either by the baffle surface or the sphere surface. Because the reflection point $\boldsymbol{r}_0$ and the direction of reflection $\boldsymbol{s}$ are known, the intersection point of the photon bundle with the baffle plane or sphere surface and the distance the photon bundle travels can be determined by applying Eq. (11). If the distance between the intersection point with the baffle plane and the y axis is less than the baffle radius r_b, it implies that the photon bundle misses the baffle and hits the baffle surface. Otherwise, the photon bundle hits the sphere surface. If the photon bundle hits the sphere surface, the distance between the intersection point and the y axis is also calculated. The photon bundle escapes the integrating sphere if the distance is less than r_d, where r_d is the radius of the detector port. If the photon bundle remains inside the sphere, a new set of θ' and ϕ' is generated. By combining θ' and ϕ' with $\boldsymbol{t}_1$, $\boldsymbol{t}_2$, and $\boldsymbol{n}$ of the corresponding surface, the new direction of reflection can be derived. Special attention shall be paid to the sign of $\boldsymbol{n}_b$. If the reflection point is to the right of the baffle surface, $\boldsymbol{n}_b$ takes positive value and vice versa. The weight of the photon bundle decreases to a fraction of $(1 - \alpha_i)$ of its former value after each time hitting the baffle or sphere surface, where α_i is the absorptance of the integrating sphere surface (sphere or baffle surface). Using the intersection point as the new reflection point, a new intersection point and distance the photon bundle travels can be determined. The process is continued until either the weight of the photon bundle is too low (e.g., <0.01) or the photon bundle escapes from the sphere. When the weight of the photon bundle is too low, a random number is generated between 0 and 1. If the random number is less than, for example, 0.2, the weight is increased by a factor of 5. Otherwise, the photon bundle is killed. This is done to avoid tracing too weak photon bundles while still conserving energy. The procedure just described is called Russian roulette, a standard Monte Carlo technique to reduce the variance of simulation. When the photon bundle escapes from the detector port, its weight and the total distance it travels inside the sphere are

recorded. The time for the photon bundle to escape the sphere can then be calculated. It is added to the photon bundle's time tag to yield a new time tag that specifies the time the photon bundle escapes the sphere.

The tallying of the photon bundle is done according to its time tag. The total weight of all photon bundles escaping the sphere during a certain time interval is calculated. It is divided by the maximum total weight of photon bundles that are generated in the same time span. The result is the fraction of laser irradiation that leaves the integrating sphere at a certain instant.

Monte Carlo Results

To validate the present Monte Carlo simulation, a steady-state result has been obtained for a relatively simple case, for which the theoretical result has been found.[4] The integrating sphere has no baffle. The diameter of the detector port is normalized against the diameter of the integrating sphere. The normalized diameter of detector port $\bar{d}$ varies from 0.484 to 9.98×10^{-2}. The sample absorptance α_s is taken as 0.5, and the sphere absorptance α_i is taken as either 0.05 or 0.1. For each Monte Carlo simulation, 2×10^4 photon bundles are generated. The fraction of laser irradiation leaving the integrating sphere obtained using Monte Carlo methods, f_m, is compared with the theoretical results f_t. The Monte Carlo and theoretical results are shown in Table 1. It can be seen that the error of the Monte Carlo simulation is within 1% for all of the cases. The error is due to the statistical scatter inherent to the Monte Carlo methods.

A transient Monte Carlo simulation is performed to find the time constant of an integrating sphere. A square wave laser pulse is simulated first. The sample absorptance is taken as 0.5, and the sphere absorptance is taken as 0.05. The diameter of the baffle is selected such that no photon bundle can escape the sphere directly. The normalized distance between the center of the sphere and the baffle surface $\bar{l}$, which is normalized against the diameter of the integrating sphere, varies from 0.25 to 0.465. The Monte Carlo results are plotted against normalized time $\bar{t}$, which is defined as tc_l/r_s, where c_l is the speed of light and r_s is the radius of the integrating sphere. Those results are curve fitted with an exponential function, $f_m(\bar{t})/f_{m0} = [1 - \exp(-\bar{t}/c_t)]$, where $f_m(\bar{t})$ is the fraction of radiation that escapes the integrating sphere at instant $\bar{t}$, f_{m0} is the steady-state result for the same geometry, and c_t is the time constant of the sphere. Typical results for an integrating sphere with normalized diameter of the detector port $\bar{d}$ of 0.198 are shown in Fig. 2, where $\bar{l}$ is 0.333 and 0.417 and the normalized diameter of the baffle is 0.168 and 0.170. It is found that the time constant is independent of the size and position of the baffle. For the geometry just described, the time constants for all of the baffle sizes and positions considered are approximately 23.2. This may be explained as follows. When the baffle is closer to the detector port, the fraction of radiation escaping the sphere at a given time is smaller. However, the fraction of radiation that leaves the integrating sphere at steady state is also smaller. Therefore, the ratio $f_m(\bar{t})/f_{m0}$ and, thus, the time constant remain the same for different baffle positions. For different sizes of detector ports, the time constant of an integrating sphere is listed in Table 2. It shows that the time constant decreases with the increase of the diameter of the detector port because it takes less bounces for a photon bundle to escape a larger detector port.

Table 1 Theoretical and Monte Carlo results

f_t	f_m	$\bar{d}$	α_i	α_s
0.2857	0.2828	0.484	0.05	0.5
0.1960	0.1975	0.348	0.05	0.5
4.573×10^{-2}	4.635×10^{-2}	0.198	0.1	0.5
2.385×10^{-2}	2.372×10^{-2}	9.98×10^{-2}	0.05	0.5

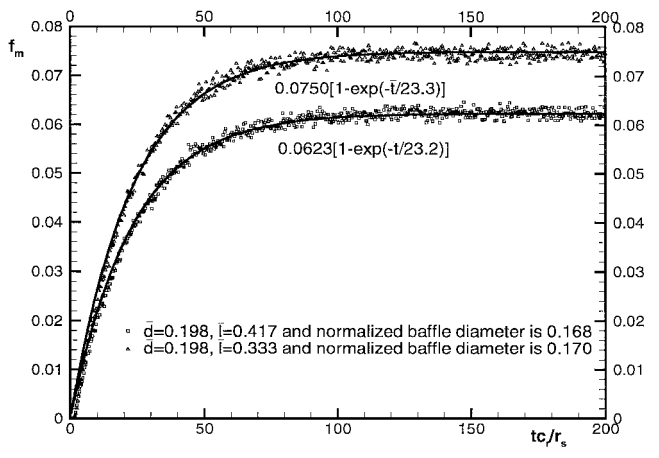

Fig. 2 Transient responses of integrating spheres to a square wave.

Table 2 Time constants of integrating spheres

$\bar{d}$	c_t
9.98×10^{-2}	27.6
0.149	24.2
0.198	23.0
0.247	21.7
0.296	20.9
0.343	20.3

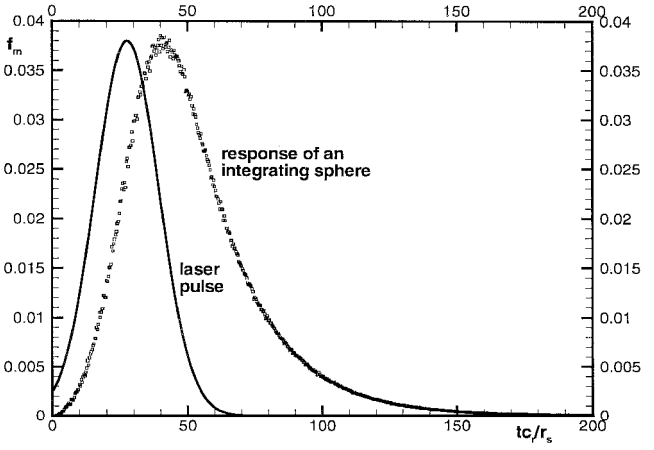

Fig. 3 Transient response of an integrating sphere to a Gaussian pulse.

A transient response of an integrating sphere to a Gaussian pulse is shown in Fig. 3. The Gaussian pulse follows $p(t) = c \exp[-a(t - t_{\max})^2]$, where c and a are constants and $t_{\max}$ corresponds to the time the laser pulse peaks. The Gaussian pulse has a normalized half-width of 27.6, which is the time constant for the integrating sphere used in the Monte Carlo simulation. For an integrating sphere of 10 cm in diameter, the half-width is 9.2 ns, which is typical for a Q-switched laser. It can be seen that the transient response of the integrating sphere lags behind the Gaussian pulse, while the pulse width is broadened by the integrating sphere as well.

Conclusion

A Monte Carlo simulation of radiation transport inside an integrating sphere is performed. A steady state, simple geometry case is tested first. The results agree well with previous theoretical results. The transient response of a square wave laser irradiation is simulated to find the time constant of the integrating sphere. It is found that the time constant of an integrating sphere does not change with the size and position of the baffle. The time constant decreases with the increase of the size of the detector port. A simulation of transient response of an integrating sphere to a Gaussian laser pulse is conducted as well. The Monte Carlo results show that the response of a typical integrating sphere significantly lags behind a typical Q-switched laser pulse, while the shape of the response agrees reasonably well with that of the pulse.